Model uncertainty in a parametric fire curve approach: a stochastic correction factor for the compartment fire load density

Florian Put[a*], Andrea Lucherini[a,b], Bart Merci[a], Ruben Van Coile[a]

[a]Department of Structural Engineering and Building Materials, Ghent University, Technologiepark-Zwijnaarde 60, Gent, Belgium, Florian.Put@UGent.be

[b]Department for Research of Fire-Safe Sustainable Environment (FRISSBE), Slovenian National Building and Civil Engineering Institute (ZAG), Slovenia.

*Corresponding author

Highlights:

- The fire severity model uncertainty is quantified by fire load correction factor
- The declared thermal inertia of the linings strongly affects the correction factor
- Application of the correction factor allows for reliability-based design

Abstract:

A commonly used approach to represent the thermal load in a compartment fire is the Eurocode Parametric Fire Curve (EPFC), which specifies gas temperatures (or rather adiabatic surface temperatures). Recognizing the significant deviations between real fires and the EPFC framework, the concept of model uncertainty is explored. This study does not aim to assess or improve the EPFC, but introduces a model uncertainty, allowing for reliability-based structural fire engineering (SFE). It presents a stochastic correction factor for the fire load density, based on the maximum temperature in steel sections. The focus is on the fire load density, but in general other parameters can be jointly taken into account as well. This correction factor considers protected and unprotected sections, incorporating variations in section factor and protection thickness. The findings reveal that the fire load density within the EPFC framework can be modified to better represent the severity of fire experiments. This approach ensures physical consistency of the obtained compartment gas temperatures, as opposed to alternative approaches for addressing the EPFC model uncertainty. While promising results are evident in this proof of concept, exploration for other types of structural elements and evaluation for structural systems is necessary before integration into design practices.

Keywords: structural fire engineering; compartment fires; fire load density; steel structures; reliability; probability of failure

1. Introduction

A structural fire design is traditionally deemed to be satisfactory when prescriptive design requirements are met. The main requirement is usually associated with fire resistance, R, and indicates the time a structural element can maintain load-bearing capacity when exposed to a

prescribed nominal heating regime, e.g. ISO 834 [1] or ASTM E119 [2]. Due to its simplicity and generality, facilitating standardization, this methodology has been adopted in many design guides and building codes (e.g. [3], [4]).

Nevertheless, standardized time-temperature curves enable homogenization and comparison, but they are not capable of representing realistic exposures for post-flashover compartment fires [5]. They are invariant and lack specific consideration of the compartment in which the fire is situated, e.g., fuel and compartment characteristics. Besides, they completely ignore the existence of a fire decay and cooling phase. Therefore, they can only be used within the boundaries of the prescriptive design paradigm. Recent research ([6]–[8]), however, has highlighted the need for adopting a holistic approach in structural fire engineering (SFE), as traditional approaches do not comprehensively ensure the load-bearing capacity of structural elements until complete fuel burnout. A commonly used method to represent natural fires is the Eurocode Parametric Fire Curve (EPFC) [9], which considers the physical parameters (e.g., the amount and nature of the fuel, the opening area and height, material properties of the linings etc.) that have a significant influence on the severity of the fire that could develop [10].

The heating phase formulation of the EPFC is frequently regarded as a derivation of the "Swedish fire curves" ([11], [12]) which involve an energy balance at the compartment enclosure for ventilation-controlled fires. In fact, the formulation of the heating phase of the EPFC has been constructed using the principles underlying the "Swedish fire curves" and was then validated against these curves [13]. Nevertheless, it was highlighted that the method is very approximate and should be used with care [14].

Although the gas temperature described by the EPFC is more correctly referred as an adiabatic surface temperature (AST) [15], [16], it does not guarantee that element temperatures, which are of primary interest for SFE, are close to those obtained in actual fire experiments. This can lead to unsafe situations as structural elements can have been designed for less severe fire conditions than the fire that is expected in reality. Likewise, it can also lead to highly overestimated fire exposure and over dimensioned structural elements, preventing the real SFE optimization process. A detailed example demonstrating this issue is provided in section 2.1. In addition, it is currently not known what model uncertainty/correction factor can be applied to allow for a reliability-based structural fire design.

To address these issues, the concept of a correction factor (in effect, a model uncertainty) is explored, with the goal of ensuring that the modelled element temperatures correspond to those from actual fire tests. The development of such a correction factor is an indispensable step in advancing towards reliability-based structural fire engineering and will allow engineers to express the confidence they have in their designs. The correction factor is applied to the fire load density in a modified version of the EPFC (mEPFC), which avoids the discontinuity inherent within the traditional EPFC formulation. The correction factor is derived so that the maximum steel temperature reached in mEPFC exposure matches the temperatures obtained considering experimental time-temperature data.

2. Limitations of EPFC

2.1 Reliability of fire severity

The severity of the EPFC for SFE becomes evident through an assessment of the steel temperature over time when subjected to both experimentally measured time-temperature data of the gas and the corresponding EPFC. Fig 1 illustrates this scenario using Cardington fire test 6, using the compartment average of the gas temperature [17]. Despite the anticipated equivalence of the EPFC's thermal impact on the steel element, the observed steel temperature is notably lower when exposed to the EPFC, in contrast to the experimentally measured gas temperatures. Considering the maximum temperature in steel profiles as a severity metric – a representation of the most critical condition for the individual structural element and employed in the EPFC validation process [10] – it becomes apparent that, in this specific case, the EPFC underestimates the severity of actual fire exposure. While acknowledging that such discrepancies may not be universal, this observation underscores the imperative of accurately quantifying the model uncertainty associated with the EPFC.

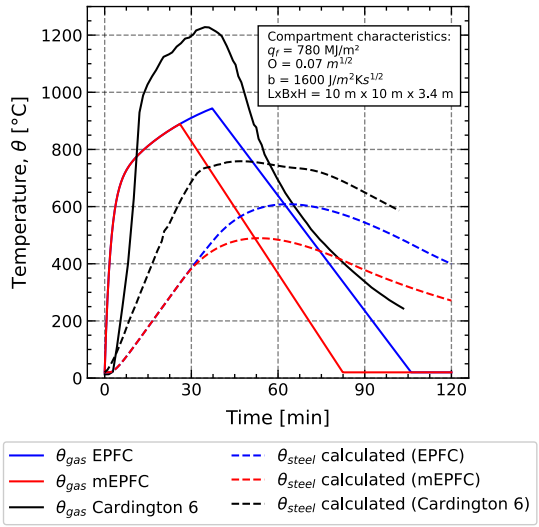

Fig 1. Gas and calculated steel temperatures for Cardington fire test 6 [17] and the corresponding EPFC and mEPFC [18] curves using a HEA200 beam protected with 2cm of SFRM [19].

2.2 Discontinuities in EPFC

The formulation of the parametric fire curve as provided in Annex A of EN 1991-1-2:2002 [9] introduces discontinuities in the maximum gas temperature at the interface between fuel- and ventilation-controlled fires, as demonstrated in Fig 2a. These discontinuities do not have a physical meaning as small variations in the opening factor or fire load density can lead to significantly different results. This also implies that for a fixed opening factor and varying fire load density (or vice versa), there will be a range of maximum temperatures that cannot be achieved. As the goal in this study is specifically to match maximum steel temperatures under exposure to experimental gas temperature data and a parametric fire curve, this phenomenon is undesirable.

The discontinuities of the EPFC have been addressed by Reitgruber et al. [18], proposing alternative formulations for the limiting opening factor, O_{lim} [$m^{1/2}$] (Eq. (1)) and the time of maximum temperature of the heating phase, t_{max} [h] (Eq. (2)):

$$O_{lim} = 0.14 \times 10^{-2} \frac{q_t}{t_{lim}} \quad (1)$$

$$t_{max} = \max\left(t_{lim}, 0.14 \times 10^{-2} \frac{q_t}{O}\right) \quad (2)$$

In these expressions q_t is the fire load density related to the total surface area of the enclosure ($q_t = q_f \cdot A_f/A_t$ with A_f the floor area and A_t the total area of the enclosure) and t_{lim} [h] is the time of maximum gas temperature in a fuel-controlled fire. This reformulation has been abbreviated in this manuscript as mEPFC.

Fig 2a and Fig 2b visualize the maximum gas temperatures for different combinations of opening factor and fire load density using the EPFC formulation and the reformulation of [18]. Although the reformulation eliminates the discontinuities in the EPFC, it also leads to different temperatures, as illustrated in Fig 2c. These temperature differences are not readily negligible with the main part of datapoints in the (O, q_f) space, having a temperature difference of 40°C or more (up to 200°C) between the two formulations. Nevertheless, the reformulation of [18] will be adopted in this research as it avoids convergence issues.

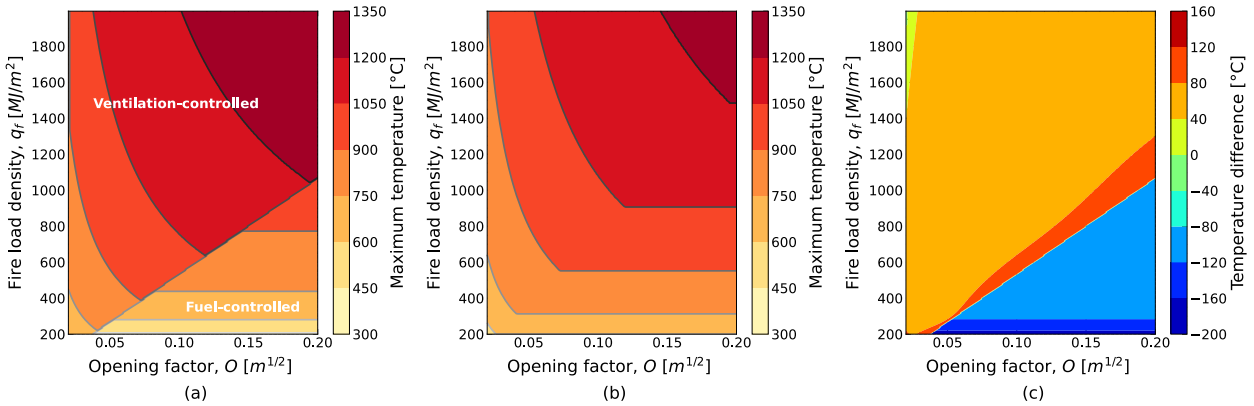

Fig 2. Maximum gas temperatures for (a) EPFC and (b) reformulation of [18] for different combinations of q_f and O, and (c) temperature difference EPFC minus reformulation. Compartment dimensions are 10 m x 10 m x 4 m and linings thermal inertia b = 1400 J/m^{2}s$^{1/2}$K.

A model uncertainty derived from the mEPFC is strictly speaking not directly applicable to the current EPFC, due to different maximum temperatures, as demonstrated in Fig 2. Nevertheless, similar results can be expected as the physical models underlying the two versions are the same, with some modifications to constants to ensure continuity. Therefore, these differences are not considered crucial for the illustration of concept in this study, although extension to the real EPFC is desirable in follow-up research. The results obtained for the mEPFC are however directly applicable to performance-based design solutions which do not rely on strict adherence to the Eurocodes.

3. Possible forms of a correction factor

The presented example in section 2.1 highlights that the application of the EPFC (or mEPFC) may not consistently yield the expected severity in real-world scenarios. Consequently, a correction, which will act as a model uncertainty, becomes essential to bridge this disparity. To establish a model uncertainty, the first step involves calculating correction factors for individual cases. This correction factor should lead to the same maximum steel temperature when applying the mEPFC model as when considering the experimentally measured gas temperatures. The maximum steel temperature is considered because it is a representation of the most critical condition for the individual structural element and has been employed in the EPFC validation process [10]. Subsequently, individual correction factors are aggregated across cases, generating a distribution of correction factors. A stochastic distribution can then be fitted to this data, leading to a

generalized correction factor. Finally, a conservative value can be derived from the generalized correction factor, resulting in a design value. This approach is visually illustrated in Fig 3. In addition, such model uncertainty can be implemented in various manners. The advantages and disadvantages of these manners are discussed below.

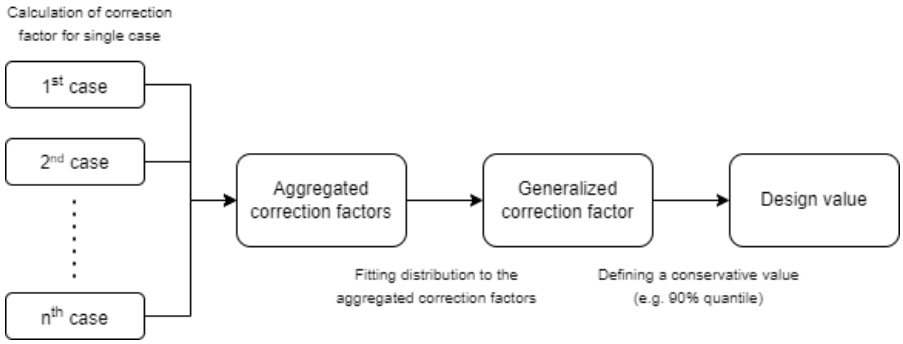

Fig 3. Schematic approach to developing a model uncertainty.

3.1 Correcting gas temperature directly

The correction can be directly applied to the gas temperature calculated by the mEPFC, which is applied as an AST within SFE calculations. This could be done considering either a multiplicative factor or an additive term, as expressed in Eq. (3) and (4) respectively.

$$T_{g,corr} = T_g \cdot \eta \quad (3)$$

$$T_{g,corr} = T_g + \eta \quad (4)$$

where $T_{g,corr}$ is the corrected gas temperature in [°C], T_g is original gas temperature and η is the correction factor or term, depending on whether it is multiplicative or additive. Note that the magnitude and dimension for the correction term will necessarily differ between both formulations. The additive term is expressed in [°C], while the multiplicative factor would be dimensionless.

Implementing such an approach is straightforward, yielding results that are intuitively clear. However, the use of a multiplicative factor introduces challenges, particularly when it is unbounded. It can lead to excessively high or unrealistically low temperatures after adjustment with the stochastic correction factor. For instance, using a lognormal multiplicative correction factor with a mean value of 1.1 and a coefficient of variation of 0.3 to adjust a maximum mEPFC gas temperature of 1000°C would result in a 2.4% probability of the corrected gas temperature exceeding 1800°C. The same general issue holds for an additive term. Even values below zero would be possible, depending on the stochastic distribution. For instance, a normal additive correction factor with a mean value of 100 degrees and a standard deviation of 50 degrees would have a 0.8% probability of yielding a negative temperature when starting from ambient temperature (20°C). While one potential solution involves making the correction factors temperature-dependent to mitigate errors at low temperatures and ensure sufficient correction at higher temperatures, this greatly increases complexity. Given the physical constraints that should be placed on the corrected gas temperatures, these approaches are not preferable.

3.2 Correcting the input parameters of the mEPFC model

Alternatively, the correction can be applied to the input parameters of the mEPFC model. This approach offers the advantage of maintaining temperature bounds determined by the mEPFC's models and equations, preventing the occurrence of excessively high or even negative temperatures in certain scenarios. The mEPFC (like the traditional EPFC) has only two degrees of freedom [5], [8]. Thus, in the following the two main input parameters of the mEPFC are considered, being the fire load density and the opening factor. The correction can be applied to either parameter individually or to both simultaneously, and the optimal choice is sought. Therefore, a case study will be used, considering an HEB400 I-profile. The section is protected with 2 cm of SFRM and the material properties are the mean values of the models provided in [19]. The section is exposed to experimentally measured gas temperatures from Cardington fire test 6 [17] and the corresponding mEPFC. The input parameters are a fire load density of 680 MJ/m², an opening factor of 0.07 $m^{1/2}$, a thermal inertia of the linings of 1600 $J/m^2Ks^{1/2}$, a floor area of 12 m by 12 m and a height of 3.4 m.

To illustrate the general influence of both the fire load density and opening factor in the mEPFC framework, the maximum steel temperatures for the presented case study are investigated for different combinations of these parameters. The calculation of the steel temperature is done through the lumped mass approach of EN 1993-1-2:2005 [20], as described in section 4.2. The results, presented in Fig 4, illustrate that the influence of the opening factor is significantly smaller than the influence of the fire load density. For a fixed value of the opening factor, a change in fire load density will almost always allow for reaching the desired maximum temperature, except for very low values of the opening factor. This is due to the wide range of fire load densities that EN 1991-1-2:2002 allows. For a fixed fire load density, however, the range of temperatures that can be reached by varying the opening factor is very limited. In many cases, it is not even possible to reach the desired temperature considering the acceptable range of opening factors recommended in EN 1991-1-2:2002 [9], which is from 0.02 to 0.2 $m^{1/2}$.

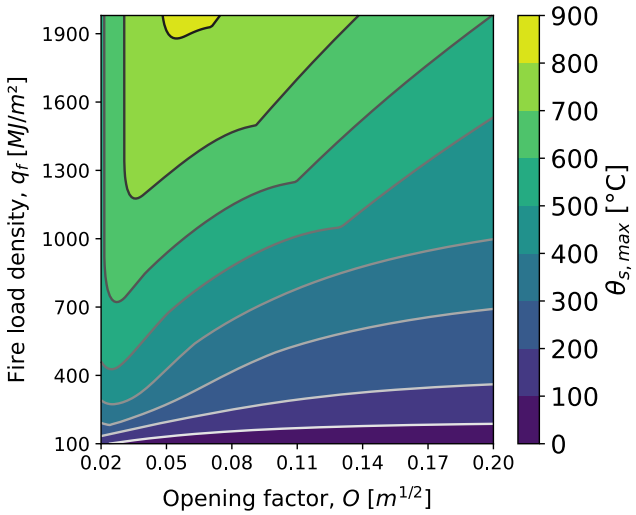

Fig 4. Maximum steel temperatures that can be reached for different combinations of fire load density and opening factor using a HEB400 profile protected with 2 cm of SFRM.

3.2.1 Correcting the opening factor

In the presented case study, the maximum steel temperature achieved during exposure to experimentally measured gas temperatures is 712°C. The mEPC is now used considering the

declared fire load density of 680 MJ/m², and the opening factor is varied with the goal of obtaining the same maximum steel temperature of 712°C. However, the fire curves in Fig 5a demonstrate a limited impact of varying the opening factor on the maximum temperature obtained. Notably, no physical solution is found within the bounds specified by EN 1991-1-2:2002 [9], as indicated in Fig 5b. Even if only cases would be considered where a solution is found, conservatism lacks a clear definition for the opening factor, where a higher opening factor could lead to either more intense burning (if ventilation-controlled) or lower temperatures (if fuel-controlled). Consequently, applying the correction factor solely to the opening factor is not the preferred option.

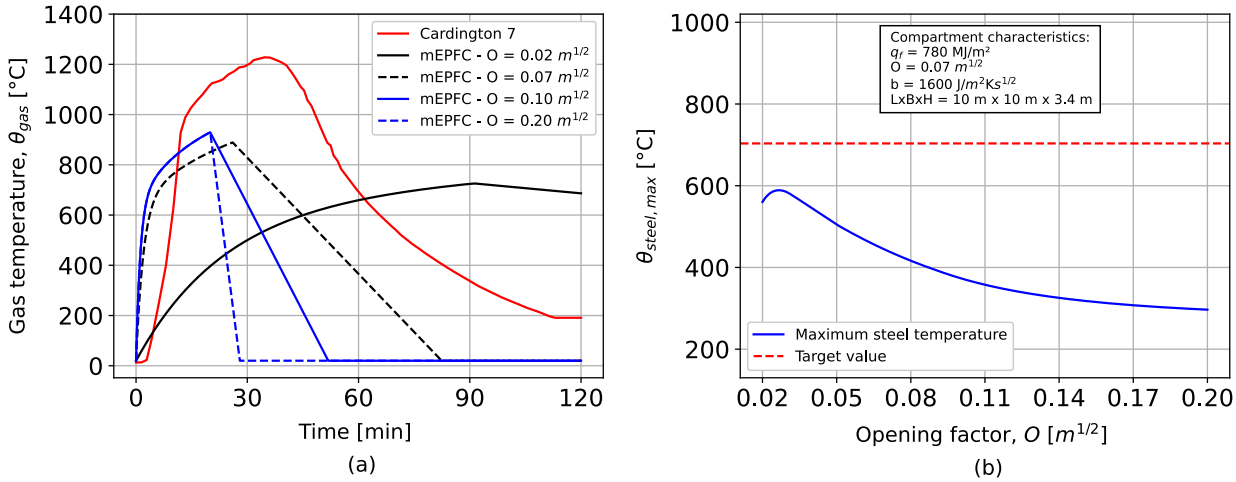

Fig 5. Case study considering a HEB400 profile with 2 cm of SFRM with (a) the experimental fire curve and different mEPFC curves with varying opening factor and (b) the maximum achievable temperatures within the EN 1991-1-2:2002 [9] bounds.

3.2.2 Correcting the fire load density and opening factor simultaneously

The correction factor can also be applied to the fire load density and opening factor simultaneously. This approach requires the definition of a second correction criterion besides the maximum steel temperature as multiple combinations of fire load density and opening factor may result in the same maximum steel temperature. Although defining a second criterion is possible (e.g., requiring that the maximum steel temperature is achieved at the same time as when using the experimental data), it highly complicates the definition of a correction factor as eventually two stochastic distributions will be obtained, following the approach from Fig 3. Furthermore, when applying a second criterion, often no solution will exist.

3.2.3 Correcting the fire load density

This leaves the fire load density as the last option to apply the correction factor to. Employing the declared opening factor (0.07 $m^{1/2}$), the same maximum temperature is attainable by increasing the fire load density from 680 MJ/m² to 1404 MJ/m² (detailed methodology in Fig 6), demonstrating that a stochastic correction factor for the fire load density is feasible. This format for considering the fire severity model uncertainty has the advantage that it maintains the simplicity of a single correction factor. Besides, conservatism can be clearly defined for this parameter because an increase in fuel mass will either lead to a longer fire (if ventilation-controlled) or a more intense fire (if fuel-controlled). In addition, EN 1991-1-2:2002 [9] does not put explicit boundaries on the

fire load density, facilitating convergence in the maximum steel temperatures (i.e., when evaluating the correction factor for individual cases, as described in Fig 3). Considering the above, it is concluded that efforts for the development of a correction factor should focus on the fire load density as an isolated parameter first.

4. Correction factor for the fire load density in structural design

4.1 Methodology to correct mEPFC severity

The stochastic correction factor for the fire load density is determined based on the maximum temperature in steel sections when exposed to experimentally measured temperatures on the one hand and the mEPFC on the other hand. The section temperature is calculated using the lumped mass capacitance approach of EN 1993-1-2:2005 [20]. First, the declared fire load density q_f of the experiments is used as input for the mEPFC calculation. If the maximum section temperatures are not in agreement, the fire load density is adjusted until convergence is obtained. The fire load density inducing convergence is called the equivalent fire load density and is denoted $q_{f,eq}$. The formulation for the correction factor η is given in Eq. (5).

$$\eta = \frac{q_{f,eq}}{q_f} \tag{5}$$

Both protected and unprotected steel sections are considered. The protected sections are covered with a sprayed fire-resistive material (SFRM). The material properties of the SFRM are taken as the mean values of the models provided in [19], whereas the steel thermal properties are taken from EN 1993-1-2:2005 [20]. The methodology presented here, which is schematically visualized in Fig 6, can be extended to other fire protection materials in follow-up research.

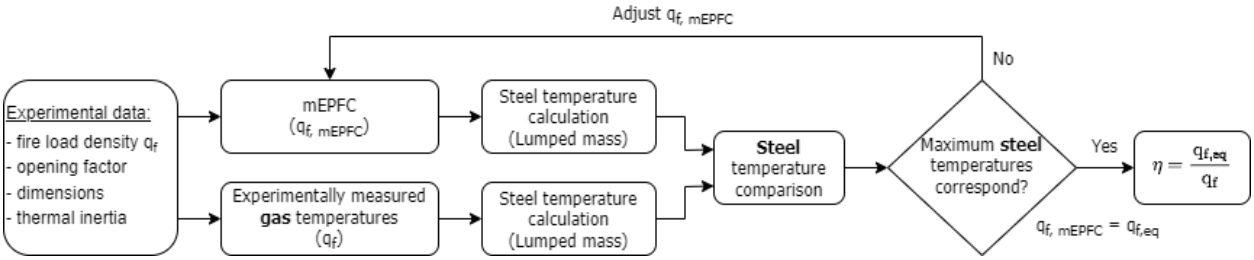

Fig 6. Schematic overview of the applied methodology.

4.2 Eurocode 3 lumped mass capacitance calculation method

The lumped mass capacitance calculation method of EN 1993-1-2:2005 [20] assumes a uniform temperature distribution in a cross-section and provides separate formulations depending on whether the steel section is protected or not. For unprotected sections, the temperature increase per unit time is given by Eq. (6):

$$\Delta\theta_{a,t} = k_{sh} \frac{A_m/V}{c_a \rho_a} \dot{q}_{net} \Delta t \tag{6}$$

where $\Delta\theta_{a,t}$ [°C] is the steel temperature increase, k_{sh} [-] is the section's shadow factor, A_m/V [m^{-1}] is the section factor, c_a [J/kgK] and ρ_a [kg/m^3] are respectively the specific heat and density of steel, $\dot{q}_{net}$ [W/m^2] is the net heat flux per unit area and Δt [s] is the time interval. The shadow factor, k_{sh}, for non-nominal fire exposures is calculated as the ratio of the box value of the section

factor and the real section factor, $[A_m/V]_b$ /$[A_m/V]$. Substituting the elaborated version of the shadow factor in Eq. (6), eliminates the dependency of $\Delta\theta_{a,t}$ on A_m/V, as indicated in Eq. (7).

$$\Delta\theta_{a,t} = \frac{[A_m/V]_b}{c_a\rho_a}\dot{q}_{net}\Delta t \tag{7}$$

When the steel profile is covered by a protective material, both the effect of the thermal insulation and the additional heat capacity should be considered. A simple approximation is to lump one-third of the heat capacity of the insulation to the steel heat capacity and to add a term to account for the time delay [21]. This approach has also been adopted in EN 1993-1-2:2005, provided in Eq. (8). As this approach is commonly used and leads to satisfying results, it is also adopted here. The last (exponential) term of Eq. (8) accounts for the time delay induced by the protective material and the term $\Phi/3$ in the denominator lumps one-third of the heat capacity of the protective material to the steel section heat capacity. The factor 10 in the exponential term was based on a comparison with accurately calculated temperatures [21].

$$\Delta\theta_{a,t} = \frac{\lambda_p A_p/V\cdot(\theta_{g,t}-\theta_{a,t})}{d_p c_a\rho_a(1+\frac{\Phi}{3})}\Delta t - \left(e^{\frac{\Phi}{10}}-1\right)\Delta\theta_{g,t} \qquad \text{with } \Phi = \frac{c_p\rho_p}{c_a\rho_a}d_p A_p/V \tag{8}$$

In these expressions, (in addition to the formulation for unprotected members) λ_p [W/mK], c_p [J/kgK] and ρ_p [kg/m^3] are respectively the thermal conductivity, the specific heat and the density of the protective material, d_p [m] is the thickness of the protective material, A_p/V [m^{-1}] is the section factor for protected steel members and $\Delta\theta_{g,t}$ [°C] is the increase of the gas temperature during the time interval Δt [s], taken as 0.5 s for all calculations in the presented work. It should be noted that the fire and exposed surface temperatures are assumed equal in this formulation, while this is not the case for the unprotected steel sections. This implies that the inverse of the total heat transfer coefficient (convective and radiative heat transfer between gas and protective material) is assumed negligible compared to the (conductive) heat resistance of the insulation [21], which is a fair assumption for well-insulating materials. Additionally, Φ should not exceed 1.5 to maintain the assumption that there is no heat storage in the insulation material [22]. To satisfy this requirement for the insulation material considered here, the maximum insulation thickness should not exceed 0.05 m.

4.3 Experimental data

The fire load density correction factor was defined in Eq. (5). Therefore, the experimental data used should have a clear description of (i) the fire load density; (ii) the opening factor; (iii) the thermal inertia; and (iv) the compartment dimensions. A set of exemplar experiments fulfilling these requirements are selected from the literature and the respective parameters and references are listed in Table 1. The experimental cases have been selected as representative examples. They do not aim at being generally representative of post-flashover compartment fire. The measurements were conducted using bare-bead thermocouples and are generally not directly applicable as AST, which can only be measured with an idealized plate thermometer [21]. Nevertheless, research has indicated that the difference between the two measuring devices becomes insignificant for longer fire durations (+10 minutes) [23].

The experimental time-temperature curves are provided in Fig 7 and incorporate the average values of the temperatures measured during the experiment, which was also the approach followed in the validation of the EPFC [10]. Although models often assume the post-flashover compartment to

have one temperature (one-zone assumption), experimental measurements will show temperature differences based on the location within the compartment. In addition, measurements also come with a certain accuracy. As the choice of the experimental time-temperature curves is closely related to the estimations of the correction factor, quantification of the uncertainty is relevant for accurate predictions of the stochastic correction factor. Therefore, exploring the implications of measurement errors is highlighted as a topic for follow up research.

Table 1. Details on the large-scale experimental data.

	Fire load density	**Opening factor**	**Thermal inertia**	**Length**	**Width**	**Height**	**Ref.**
Cardington 1	680 MJ/m²	0.1 $m^{1/2}$	1600 $J/m^2s^{1/2}K$	12 m	12 m	3.4 m	[17]
Cardington 2	680 MJ/m²	0.1 $m^{1/2}$	720 $J/m^2s^{1/2}K$	12 m	12 m	3.4 m	
Cardington 3	680 MJ/m²	0.1 $m^{1/2}$	720 $J/m^2s^{1/2}K$	12 m	12 m	3.4 m	
Cardington 4	680 MJ/m²	0.07 $m^{1/2}$	720 $J/m^2s^{1/2}K$	12 m	12 m	3.4 m	
Cardington 5	680 MJ/m²	0.078 $m^{1/2}$	720 $J/m^2s^{1/2}K$	12 m	12 m	3.4 m	
Cardington 6	680 MJ/m²	0.07 $m^{1/2}$	1600 $J/m^2s^{1/2}K$	12 m	12 m	3.4 m	
Cardington 7	680 MJ/m²	0.07 $m^{1/2}$	1600 $J/m^2s^{1/2}K$	12 m	12 m	3.4 m	
Cardington 8	680 MJ/m²	0.1 $m^{1/2}$	1600 $J/m^2s^{1/2}K$	12 m	12 m	3.4 m	
Ostrava	1039 MJ/m²	0.04 $m^{1/2}$	1059 $J/m^2s^{1/2}K$	3.8 m	5.95 m	2.78 m	[24]
Ulster	587 MJ/m²	0.04 $m^{1/2}$	1104 $J/m^2s^{1/2}K$	15.6 m	9.2 m	2.88 m	[25]

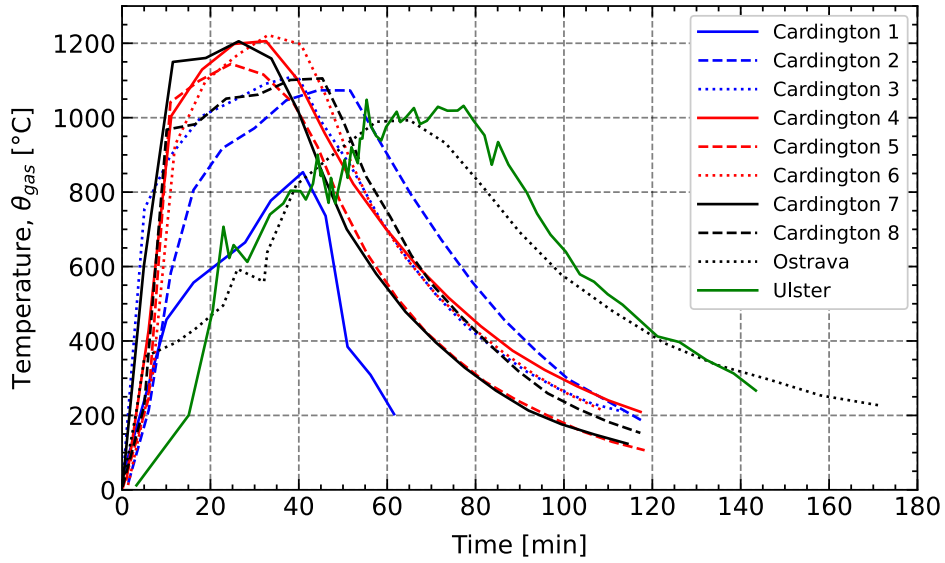

Fig 7. Experimental time-temperature curves (compartment averages).

5. Stochastic correction factors based on steel sections

A total of 1470 cases are considered to calculate the equivalent fire load density and resulting stochastic correction factor: 550 protected steel members and 810 unprotected members. The dataset for protected steel sections is based on 10 experimental time-temperature curves, 11 section factors in the range from 40 up to 440 m^{-1} (i.e., 40, 80, 120… m^{-1}) and 5 insulation thicknesses (i.e. 1 to 5 cm, to satisfy the Φ requirement), resulting in a total of 550 cases. The dataset for unprotected steel sections is based on the same experimental time-temperature curves and 81 (box) section factors in the range from 40 up to and including 440 m^{-1} (i.e., 40, 45, 50, 55… m^{-1}). The

range of the section factors was determined based on the combination of the normal and boxed values of HEA, HEB, HEM and IPE profiles.

Based on the frequency of occurrence of the calculated correction factors, the best fitting distribution is determined using the Akaike Information Criterion (AIC), as in [26]. The AIC evaluates how well a model represents the data onto which it was fitted. It is a comparative measure, in the sense that the distribution with the lowest AIC for a given problem constitutes the best fit. The models (distributions) that have been considered are lognormal, gamma, and inverse Gauss. Distributions yielding probabilities for negative values of the stochastic correction factor have been eliminated upfront because such values are illogical as they would imply negative fire load densities. For each distribution, the number of independent variables in the model is 2 (mean and standard deviation of the dataset).

5.1 Unprotected steel sections

The visualization of the results in Fig 8a shows that for unprotected steel sections, the correction factor for the fire load density is chaotic, without a clear pattern. This is also confirmed by the mean (μ_η=2.94) and standard deviation (σ_η=2.95) of the dataset. Instead of a continuous distribution, multiple discrete peaks can be observed. As a result, the overall agreement of the models with the experimental data is poor.

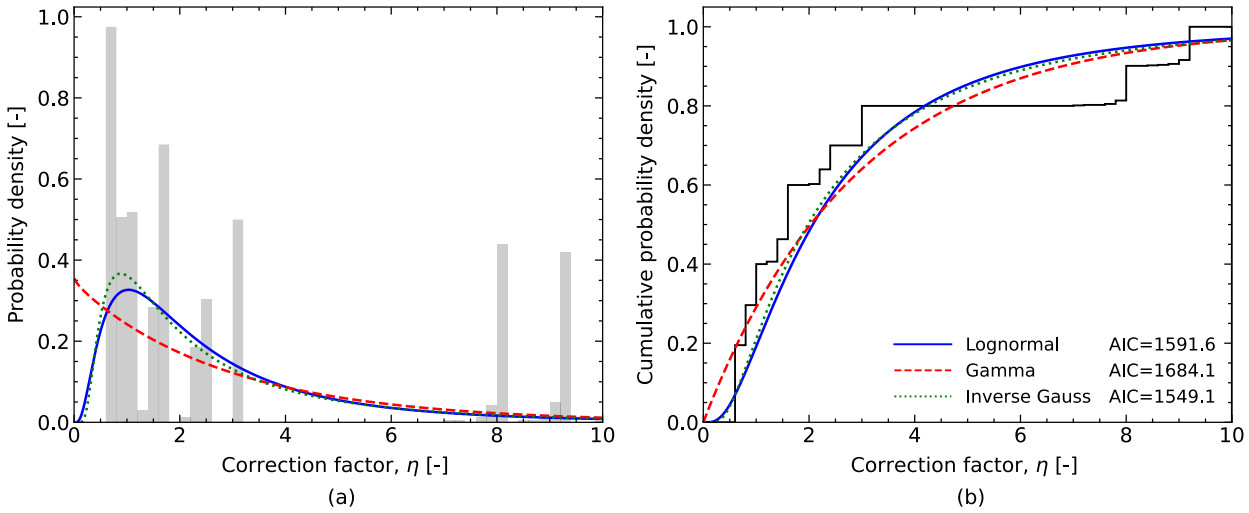

Fig 8. Comparison of the calculated correction factors for unprotected steel sections with fitted distributions using (a) PDF and (b) CDF.

The calculation method of the temperature increase of the steel section (Eq. (7)) depends on the box section factor. Fig 9 visualizes how the calculated correction factor varies with the box section factor. The calculated correction factor is relatively independent of the box section factor, except for the lower-end values. Nevertheless, it is obvious from Fig 9 that the experimental data used to calculate the equivalent fire load density has a big influence. Some sets of experimental data lead to high values for the correction factor (e.g. Cardington 6 and 7), whereas other sets lead to correction factors around or below unity (e.g. Cardington 5).

Given that the box section factor was the only parameter that was varied in Eq. (7), the results of Fig 9 can be used to explain the peaks in Fig 8. The discrete peaks relate to individual tests, which is caused by the relationship between the gas temperature and the steel temperature for unprotected

sections. The steel temperature is known to closely follow the gas temperature, especially when the section factor is sufficiently high [10]. The time aspect is less relevant. Correcting the maximum steel temperature is in such cases almost equivalent to directly correcting the gas temperature. Given that the number of experimental datasets is limited, this results in discrete peaks in a histogram.

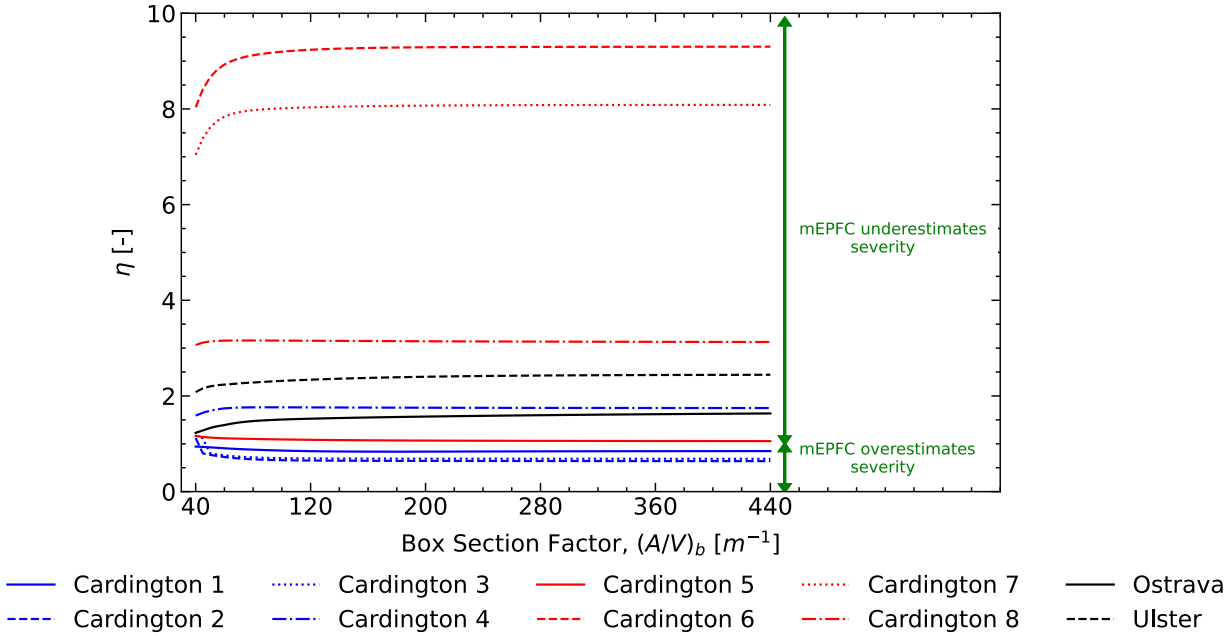

Fig 9. Influence of box section factor on the correction factor for unprotected steel sections.

The experimental datasets entailing high correction factors are primarily the sets from Cardington tests 6 and 7, whereas Cardington test 8 and the test from Ulster University demonstrate similar behavior but to a lesser extent. Table 1 reveals that the principal similarity among these curves lies in the high thermal inertia of the linings, a measure of the temperature response of a body during heat transfer, as defined in Eq. (9). Also Cardington fire test 1 has a high value for the thermal inertia of the linings, but given that this test did not progress into full flashover as the other tests did (see Fig 7), it cannot be considered fully reliable.

$$b = \sqrt{k\rho c} \tag{9}$$

where b is the thermal inertia [J/m²Ks$^{1/2}$], k is the thermal conductivity of the material [W/mK], ρ is the density of the material [kg/m³] and c is the specific heat [J/kgK].

When the thermal inertia of the linings is high, the EPFC (and mEPFC) considers that more energy is lost to the linings. This energy can no longer be used to increase the gas temperature. Hence, the temperature predicted by the EPFC is lower when the thermal inertia is high. Nevertheless, this influence is not noticeable in the experimentally measured time-gas temperature curves of Fig 7. Cardington tests 6 and 7 reach, for example, higher temperatures than Cardington test 5, although it has a lower thermal inertia. Therefore, the maximum steel temperature depends less on the thermal inertia when based on experimental data compared to when the EPFC is used. Consequently, a higher correction factor is obtained with increasing thermal inertia.

5.2 Protected steel sections

The calculated correction factors for protected steel sections exhibit a much more regular behavior than the correction factors based on unprotected steel sections. As indicated with the histogram in Fig 10a, the highest probability density is found for correction factors around 1.75. This is in line with the mean (μ_η=1.74) and standard deviation (σ_η=0.80) of the dataset. Using the AIC, the lognormal and inverse Gauss distributions provide similar agreement. In addition, the agreement between these distributions and the experimental data in Fig 10 is good, as illustrated by both the PDF (Fig 10a) and CDF (Fig 10b) plots. Both the peak probability density and the extremes of the distribution are well represented.

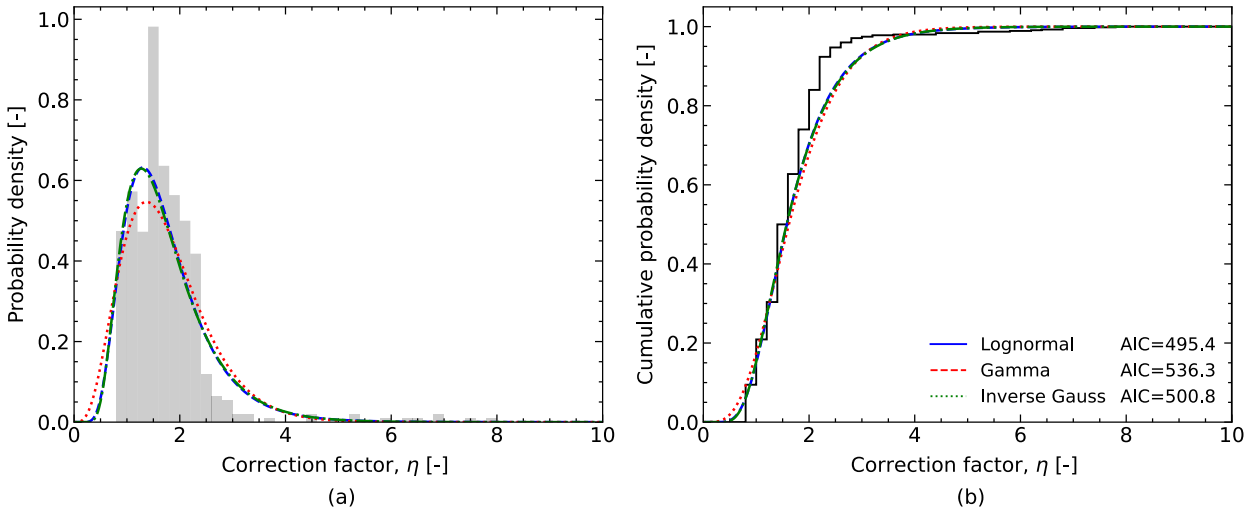

Fig 10. Comparison of the calculated correction factors for protected steel sections with fitted distributions using (a) PDF and (b) CDF.

For protected steel sections, two parameters will affect the steel section temperature, being the insulation thickness and the section factor. Their influence on the calculated correction factor is reported in Fig 11a and Fig 11b, respectively. For both parameters, the median value, i.e., the center line of the boxplot, remains approximately constant. For the section factor, the first and third quartiles (indicated by whiskers) separate further from each other as the section factor increases, indicating a larger spread on the calculated correction factors. For the insulation thickness, the opposite is valid.

Similar to the unprotected sections, the outliers originate from Cardington fire tests 6 and 7, indicating that the thermal inertia is also important for protected steel sections. These outliers are found mainly for low insulation thicknesses and high section factors and even increase with the section factor. For these cases, the same logic as for unprotected sections can be applied. The outliers occur most frequently for low insulation thicknesses, as this is the closest to the unprotected case. Furthermore, a higher section factor represents a thinner section, which will follow the gas temperature more closely. The influence of the section factor is bigger than for unprotected sections due to the time delay introduced by the thin layer of insulation material.

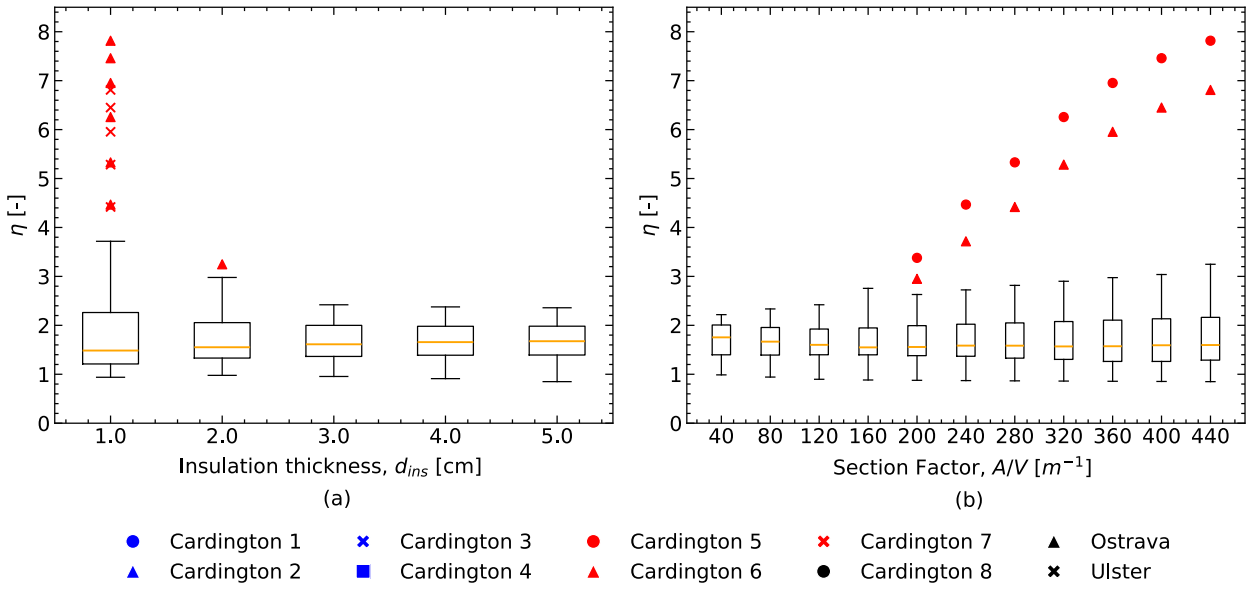

Fig 11. Influence of (a) insulation thickness and (b) section factor on the correction factor for the fire load density.

5.3 Protected and unprotected steel sections

Combining the results for protected and unprotected steel sections in a single dataset, the histogram provided in Fig 12a is obtained. The more consistent data from protected steel sections are completed with the less consistent data from unprotected steel sections. This mainly affects the spread on the data as compared to the dataset for protected steel sections, as confirmed by the mean (μ_η=2.45) and standard deviation (σ_η=2.41). Again, the lognormal, and inverse Gauss distributions produce the best fit for the experimental data, as illustrated using the AIC in the legend of Fig 12. It should be noted that these results depend on the ratio of unprotected to protected cases, with the unprotected cases being more numerous and thus having a more pronounced effect on the total dataset.

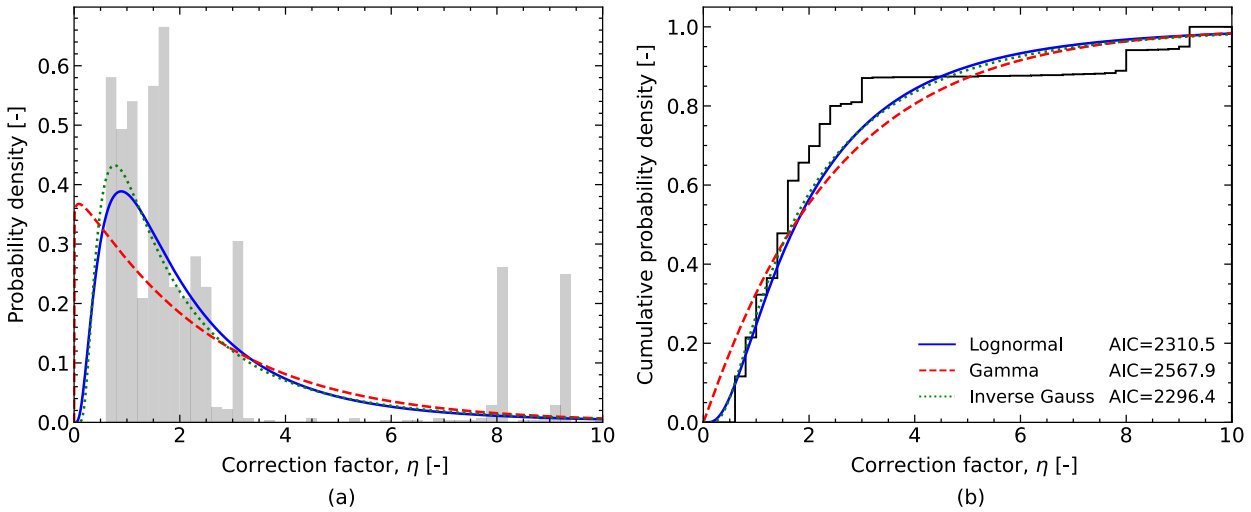

Fig 12. Comparison of the calculated correction factors for both protected and unprotected steel sections with fitted distributions using (a) PDF and (b) CDF.

6. Discussion

6.1 Maximum steel temperature as metric

The proposed methodology provides a correction factor, to be multiplied with the fire load density, by matching the maximum steel section temperatures between exposure to mEPFC and exposure to experimental time-temperature data. The maximum steel temperature univocally defines a quantification for the severity of the fire exposure as experienced by structural steel elements. Nevertheless, this approach does not ensure a good agreement between the two steel temperature-time curves during the entire fire event. Thermally-induced restraint forces may trigger different failure modes. The development of such loads are, however, case-specific and it would be hard to draw general conclusions from such results. Hence, the focus is placed on the maximum steel temperature, aligning with the general point of lowest capacity - an approach consistent with the methodology employed within the project that introduced and calibrated the EPFC [10].

6.2 Importance for structural fire performance

The application of a stochastic correction factor for the fire load density to enhance the agreement in fire severity between the mEPFC and experimentally measured gas temperatures is only relevant for SFE when it affects the structural performance. The structural performance is largely related to the properties of building materials, which generally reduce with elevating temperatures. Noticeable reductions, however, will only occur from a certain temperature onwards. For structural steel, for example, available models (e.g., [20], [27]) predict that the yield strength starts decreasing when the material has reached a temperature of approximately 400°C while the modulus of elasticity gradually decreases from 100°C onwards [20]. The sensitivity of structural performance to fire exposure thus depends on the building material, but also on the failure mode (e.g. compressive failure vs. global buckling). Nevertheless, it is largely related to temperature. In this regard, Fig 13 indicates the maximum temperatures obtained for the cases in section 5. It can be observed that for unprotected sections, the maximum temperatures are very high, generally exceeding the abovementioned thresholds. For protected sections, the maximum temperature is significantly lower, but the 400°C threshold is also exceeded for most of the cases.

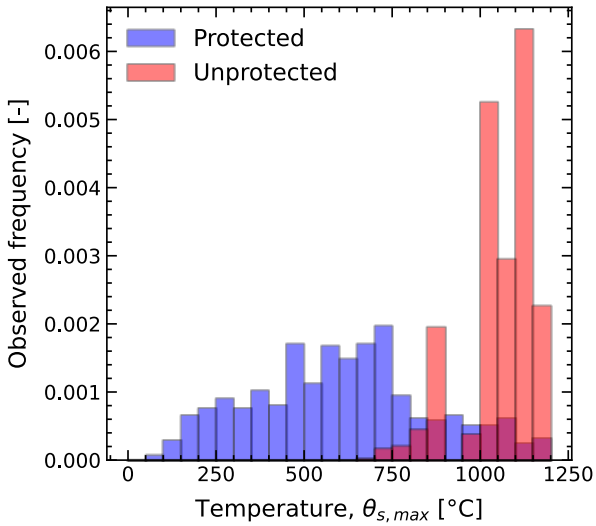

Fig 13. Histogram displaying the maximum temperature distribution for protected and unprotected steel sections, obtained from the results in section 5.

7. Illustration of the methodology

The impact of the stochastic correction factor is illustrated, using the PDF of section 5.3 (i.e., using all the data for protected and unprotected steel sections) considering two examples: an office with a protected steel section and an unprotected steel section. Both examples consider a simply supported, 3 m tall column constructed with a HEA200 profile. These simple examples considering isolated members are chosen to easily illustrate the methodology.

The protected column is covered with 20 mm of SFRM (corresponding to 90 min fire resistance) of which the temperature-dependent properties are provided in [19] (mean values are used). To model the reduction in yield strength and modulus of elasticity, the values provided in EN 1993-1-2:2005 [20] are adopted. Information on the stochastic variables in the analysis is provided in Table 2. Two failure modes are considered for the column, i.e., yielding of the steel (i.e., purely compressive failure) and global buckling. The failure mode at ambient conditions is global buckling and the resistance of the column is 307.7 kN, considering purely axial loading. The results, visualized in Fig 14 and Fig 15, are based on 10^5 realizations.

Table 2. Stochastic variables for the analyzed steel column.

Stochastic variables	**Distribution**	**Mean**	**St. dev.**
Material properties [28], [29]			
Yield strength, $f_{y,20}$ (S355)	Lognormal	393.5 MPa	25.4 MPa
Modulus of elasticity, E	Deterministic	210 GPa	-
Fire loading [9], [30]			
Fire load density, q_f	Gumbel	420 MJ/m²	126 MJ/m²
Correction factor fire load density, η	Inverse Gauss	2.45	2.41
Opening factor, O	Deterministic	0.08 $m^{1/2}$	-
Random parameter for O, ζ (following the JCSS Probabilistic Model Code [30], see Eq. (10))	Truncated lognormal (cut off at ζ=1)	0.2	0.2
Compartment characteristics			
Dimensions (L x W x H)	Deterministic	20 m x 15 m x 3m	-
Thermal inertia, b	Deterministic	1400 J/m²$s^{1/2}$K	-

$$O = (1 - \zeta)\, O_{max} \quad (10)$$

where O is the opening factor [$m^{1/2}$], ζ is a realization of the truncated lognormal distribution from Table 2 and O_{max} is the physical maximum of the opening factor.

Fig 14a demonstrates that the inclusion of the correction factor has an influence on the critical capacity of protected columns, but the reduction remains relatively limited. Before introduction of the correction factor, the maximum steel temperature did not exceed 100°C (Fig 15a), which acts as the threshold for the reduction in elastic modulus. Due to introduction of the correction factor, higher temperatures in the steel elements are obtained, exceeding the 100°C threshold, and resulting in a lower elastic modulus. The critical resistance of the column is affected. Nevertheless, the temperatures still remain relatively low with only extraordinary cases exceeding a maximum steel temperature of 200°C, at which point the elastic modulus has reduced only by 10%. Given

that the maximum temperatures remain below 400°C, the compressive strength of the steel remains unaffected.

The incorporation of the stochastic correction factor is more influential for unprotected steel columns. As temperatures can easily exceed 100°C when no protection is applied, the critical resistance is generally affected by the incorporation of the correction factor (though not always, as η may also be below 1). In many cases even the 400°C threshold (yield strength) is exceeded, meaning that also the compressive strength is affected.

Incorporating the stochastic correction factor results in an increased occurrence frequency of low capacities, emphasizing its importance in safely estimating the fire performance of structures.

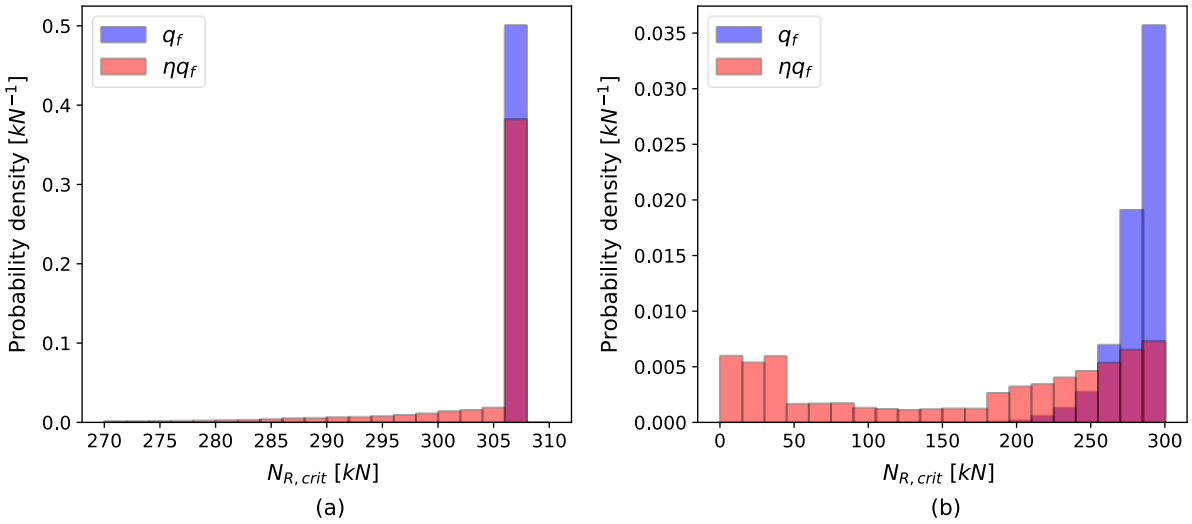

Fig 14. Probability density for the critical resistance of a simply supported 3 m tall HEA200 column exposed to mEPFC when (a) protected with 20 mm SFRM and (b) unprotected; with and without consideration of the correction factor.

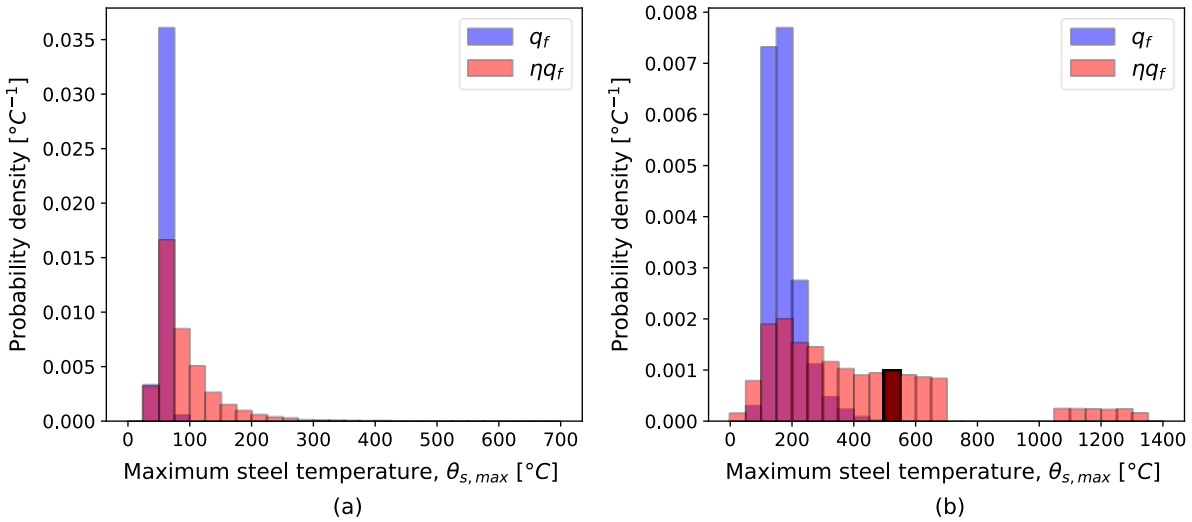

Fig 15. Change in maximum steel temperature of HEA200 profile exposed to mEPFC when (a) protected with 20mm SFRM and (b) unprotected; with and without consideration of the correction factor.

8. Recommendations for further research

Improvements can be made to enhance the applicability of the method. The following topics are listed for further developments:

- A wider range of elements. For now, focus was put on I-profiles, but the same methodology can be extended to all types of steel sections.
- Extension to other protective materials. The current study only uses a single type of protective material (SFRM). To obtain more broadly applicable results, other types of materials can be considered.
- More experimental data. The development of the correction factor was limited by the number of experiments. Additional experimental data, preferably with varying fire load density, opening factor and thermal inertia of the linings would make the method more robust.
- The current correction factor is based on the average temperature measured inside a compartment, as it was also the approach followed for the validation of the EPFC. Exploring the implications of measurement errors can further strengthen the method.
- Additional metrics. The maximum temperature in a steel section has been considered as the only metric for convergence. Introducing additional metrics, such as the time at which this temperature is reached, could potentially improve the overall agreement between the steel temperature-time curves.
- Extend to real EPFC. The current model uncertainty was based on an adapted formulation of the EPFC to avoid discontinuities at the interface between ventilation- and fuel-controlled fires. In order to make the model uncertainty applicable for the EPFC as listed within current standards, a solution needs to be found, possibly by distinguishing between fuel controlled and ventilation controlled conditions.

9. Conclusions

A stochastic correction factor for the fire load density has been determined to enhance the agreement in thermal response of steel elements considering exposure to a modified formulation of the Eurocode Parametric Fire Curve (to avoid discontinuities) and exposure to experimentally measured time-temperature curves. The maximum steel section temperature in a lumped mass capacitance approach was used as a convergence parameter. While the current focus is on the fire load density, the approach allows for simultaneous consideration of parameters. The study does not aim to assess or enhance the EPFC; instead, it introduces a model uncertainty through a stochastic approach, enabling reliability-based structural fire engineering. The correction factor, η, was found to be well above 1 (mean value μ_η=2.45 and standard deviation σ_η=2.41 for the ensemble of data used in the present study), meaning that often a higher fire load density needs to be applied to obtain the same fire severity. The influence of both the section factor and protection thickness on η was shown to be minor, whereas the declared value of the thermal inertia of the linings appeared to have a significant influence on the value of η. High thermal inertia generally leads to higher correction factors.

The structural relevance of the inclusion of a stochastic correction factor has been illustrated for the example of an office environment, considering protected (20 mm SFRM) and unprotected steel HEA200 columns, and steel yielding and global buckling as potential failure modes. In both cases, the critical resistance decreased significantly, although the effect was bigger for unprotected

sections as higher temperatures were reached. It is noted that these results are case-specific and generally depend on the insulation thickness and properties, the type of occupancy, etc. Yet, they demonstrate the importance of the stochastic correction factor as not taking this factor into account results in an assessment of the structural fire performance with little consideration of the model uncertainties and its reliability.

Acknowledgments

This research has been funded by Research Foundation of Flanders (FWO) within the scope of the research project (Grant number 1137123N) "Characterization of the thermal exposure and material properties of concrete during the fire decay phase for performance-based structural fire engineering". The second author would also like to gratefully acknowledge the financial support for the FRISSBE project within the European Union's Horizon 2020 research and innovation program (GA 952395).

References

[1] ISO, “ISO 834-1: Fire-resistance tests - Elements of building construction - Part 1: General requirements,” International Organization for Standardization, Geneva, Switzerland, 1999.

[2] ASTM, “ASTM E119-20: Standard Test Methods for Fire Tests of Building Construction and Materials,” ASTM International, West Conshohocken, USA, 2020.

[3] Royal Decree of July 7, 1994, establishing the basic standards for the prevention of fire and explosion to which buildings must comply (consolidated version). Belgisch Staatsblad, 24 Maart 2023. 2023040927.

[4] Approved Document B (fire safety)—buildings other than dwellings (2019 edition incorporating 2020 and 2022 amendments). Communities and Local Government, UK.

[5] D. Hopkin, R. Van Coile, C. Hopkin, K. LaMalva, M. Spearpoint, and C. Wade, “Design Fires and Actions,” in *International Handbook of Structural Fire Engineering*, K. LaMalva and D. Hopkin, Eds., Cham: Springer International Publishing, 2021. doi: 10.1007/978-3-030-77123-2.

[6] T. Gernay, “Fire resistance and burnout resistance of reinforced concrete columns,” *Fire Saf J*, vol. 104, no. January, pp. 67–78, 2019, doi: 10.1016/j.firesaf.2019.01.007.

[7] T. Gernay and J. M. Franssen, “A performance indicator for structures under natural fire,” *Eng Struct*, vol. 100, pp. 94–103, Oct. 2015, doi: 10.1016/j.engstruct.2015.06.005.

[8] T. Thienpont, R. Van Coile, R. Caspeele, and W. De Corte, “Burnout resistance of concrete slabs: Probabilistic assessment and global resistance factor calibration,” *Fire Saf J*, vol. 119, Jan. 2021, doi: 10.1016/j.firesaf.2020.103242.

[9] CEN, “EN 1991-1-2: Eurocode 1: Actions on structures - Part 1-2: general actions - Actions on structures exposed to fire,” European Committee for Standardization, Brussels, Belgium, 2002.

[10] J.-B. Sleich *et al.*, “Competitive steel buildings through natural fire safety concepts : final report,” EUR-OP, 2002.

[11] S. E. Magnusson and S. Thelandersson, “Temperature-Time Curves of Complete Process of Fire Development,” in *Bulletin of Division of Structural Mechanics and Concrete Construction*, vol. Bulletin 16, 1970.

[12] O. Pettersson, S. E. Magnusson, and J. Thor, “Fire Engineering Design of Steel Structures,” in *Bulletin of Division of Structural Mechanics and Concrete Construction*, vol. Bulletin 52, Lund Institute of Technology, 1976.

[13] U. Wickström, “Temperature Calculation of Insulated Steel Columns Exposed to Natural Fire,” *Fire Saf J*, vol. 4, no. 4, pp. 219–225, Jan. 1981, doi: 10.1016/0379-7112(81)90024-2.

[14] U. Wickström, “Application of the standard fire curve for expressing natural fires for design purposes,” in *Fire safety: Science and engineering*, T. Harmathy, Ed., ASTM International, 1985, pp. 145–159.

[15] A. Lucherini, B. Jovanović, R. Van Coile, and B. Merci, “Background and limitations of the Eurocode parametric fire curves, including the fire decay phase,” in *ASFE’21 Proceedings*, R. Pečenko, S. Huč, C. Chifliganec, and T. Hozjan, Eds., Ljubljana: University of Ljubljana, 2021, pp. 330–335.

[16] K. LaMalva, C. Maluk, A. Jeffers, and A. Jowsey, “Heat Transfer to Structural Elements,” in *International Handbook of Structural Fire Engineering*, 1st ed., K. LaMalva and D. Hopkin, Eds., Cham: Springer International Publishing, 2021, pp. 115–144. doi: 10.1007/978-3-030-77123-2.

[17] T. Lennon and D. Moore, “The natural fire safety concept—full-scale tests at Cardington,” *Fire Saf J*, vol. 38, no. 7, pp. 623–643, Nov. 2003, doi: 10.1016/S0379-7112(03)00028-6.

[18] S. Reitgruber, C. Di Blasi, and J.-M. Franssen, “Some Comments on the Parametric Fire Model of Eurocode 1,” in *Conference on Fire in Enclosures*, 2006, pp. 1–25.

[19] N. Elhami-Khorasani, P. Gardoni, and M. Garlock, “Probabilistic Fire Analysis: Material Models and Evaluation of Steel Structural Members,” *Journal of Structural Engineering*, vol. 141, no. 12, Dec. 2015, doi: 10.1061/(asce)st.1943-541x.0001285.

[20] CEN, “EN 1993-1-2: Design of steel structures - Part 1-2: General rules - Structural fire design,” European Committee for Standardization, Brussels, Belgium, 2005.

[21] U. Wickström, *Temperature Calculation in Fire Safety Engineering*. Cham: Springer International Publishing, 2016. doi: 10.1007/978-3-319-30172-3.

[22] Z. H. Wang and K. H. Tan, “Sensitivity study of time delay coefficient of heat transfer formulations for insulated steel members exposed to fire,” in *Fire Safety Journal*, Feb. 2006, pp. 31–38. doi: 10.1016/j.firesaf.2005.07.008.

[23] M. A. Sultan, “Performance of Different Temperature Sensors in Standard Fire Resistance Test Furnaces,” *Fire Technol*, vol. 46, no. 4, pp. 853–881, 2010, doi: 10.1007/s10694-010-0166-9.

[24] F. Wald, J. Chlouba, A. Uhlíř, P. Kallerová, and M. Štujberová, “Temperatures during fire tests on structure and its prediction according to Eurocodes,” *Fire Saf J*, vol. 44, no. 1, pp. 135–146, Jan. 2009, doi: 10.1016/j.firesaf.2008.05.002.

[25] A. Nadjai *et al.*, “Full-scale fire test on a composite floor slab incorporating long span cellular steel beams,” *Structural Engineer*, vol. 89, no. 21, pp. 18–25, 2011.

[26] B. Jovanović, N. Elhami-Khorasani, T. Thienpont, R. K. Chaudhary, and R. van Coile, “Probabilistic models for thermal properties of concrete,” University of Queensland Library, Nov. 2020. doi: 10.14264/363ff91.

[27] R. Qureshi, S. Ni, N. Elhami-Khorasani, R. van Coile, D. Hopkin, and T. Gernay, "Probabilistic Models for Temperature-Dependent Strength of Steel and Concrete," *Journal of Structural Engineering*, vol. 146, no. 6, Jun. 2020, doi: 10.1061/(asce)st.1943-541x.0002621.

[28] J. Melcher, Z. Kala, M. Holický, M. Fajkus, and L. Rozlívka, "Design characteristics of structural steels based on statistical analysis of metallurgical products," *J Constr Steel Res*, vol. 60, no. 3–5, pp. 795–808, Mar. 2004, doi: 10.1016/S0143-974X(03)00144-5.

[29] CEN, "EN 1993-1-1: Eurocode 3: Design of steel structures - Part 1-1: General rules and rules for buildings," European Committee for Standardization, Brussels, Belgium, 2005.

[30] JCSS, "Probabilistic Model Code: Part 2 - Load Models," 2001.

Figure captions

Fig 1. Gas and calculated steel temperatures for Cardington fire test 6 [17] and the corresponding EPFC and mEPFC [18] curves using a HEA200 beam protected with 2cm of SFRM [19].

Fig 2. Maximum gas temperatures for (a) EPFC and (b) reformulation of [18] for different combinations of q_f and O, and (c) temperature difference EPFC minus reformulation. Compartment dimensions are 10 m x 10 m x 4 m and linings thermal inertia b = 1400 J/m²s1/2K.

Fig 3. Schematic approach to developing a model uncertainty.

Fig 4. Maximum steel temperatures that can be reached for different combinations of fire load density and opening factor using a HEB400 profile protected with 2 cm of SFRM.

Fig 5. Case study considering a HEB400 profile with 2 cm of SFRM with (a) the experimental fire curve and different mEPFC curves with varying opening factor and (b) the maximum achievable temperatures within the EN 1991-1-2:2002 [9] bounds.

Fig 6. Schematic overview of the applied methodology.

Fig 7. Experimental time-temperature curves (compartment averages).

Fig 8. Comparison of the calculated correction factors for unprotected steel sections with fitted distributions using (a) PDF and (b) CDF.

Fig 9. Influence of box section factor on the correction factor for unprotected steel sections.

Fig 10. Comparison of the calculated correction factors for protected steel sections with fitted distributions using (a) PDF and (b) CDF.

Fig 11. Influence of (a) insulation thickness and (b) section factor on the correction factor for the fire load density.

Fig 12. Comparison of the calculated correction factors for both protected and unprotected steel sections with fitted distributions using (a) PDF and (b) CDF.

Fig 13. Histogram displaying the maximum temperature distribution for protected and unprotected steel sections, obtained from the results in section 5.

Fig 14. Probability density for the critical resistance of a simply supported 3 m tall HEA200 column exposed to mEPFC when (a) protected with 20 mm SFRM and (b) unprotected; with and without consideration of the correction factor.

Fig 15. Change in maximum steel temperature of HEA200 profile exposed to mEPFC when (a) protected with 20mm SFRM and (b) unprotected; with and without consideration of the correction factor.